Journal of Non-Crystalline Solids 330 (2003) 174–186

Nanocrystallization of fresnoite glass. I. Nucleation and growth kinetics

A.A. Cabral [a,*], V.M. Fokin [1], E.D. Zanotto [b], C.R. Chinaglia [b]

[a] *Department of Exact Sciences, Federal Center for Technological Education, 65025-001 São Luis, MA, Brazil*
[b] *DEMa-Federal University of São Carlos, P.O. Box 676, São Carlos (SP) 13565-905, Brazil*

Received 27 January 2003

Abstract

We determined the internal nucleation, crystal growth and overall crystallization kinetics of fresnoite crystal ($2BaO \cdot TiO_2 \cdot 2SiO_2$) in an almost stoichiometric fresnoite glass. Due to the extremely high nucleation rates ($\sim 10^{17}$ $m^{-3}\,s^{-1}$) that limit the maximum crystal size to $\sim$700 nm the nucleation densities and crystal sizes were estimated by scanning electron microscopy (SEM). The volume fraction crystallized was measured by X-ray diffraction. The nucleation rates obtained directly from SEM measurements reasonably agree with those calculated from the combination of overall crystallization with crystal growth kinetics. The activation enthalpies for viscous flow, transport of structural units across the nucleus/melt interface (nucleation) and crystal growth: ΔH_η, ΔH_τ and ΔH_U respectively, follow a similar trend to that observed for other stoichiometric silicate glasses that nucleate internally: $\Delta H_\eta = 294 > \Delta H_\tau = 87 > \Delta H_U = 61$ kJ/mol. Fresnoite glass displays the highest internal nucleation rates so far measured in inorganic glasses. These rates are comparable to some metallic glasses and can lead to nanostructured glass-ceramics.

1. Introduction

Crystal nucleation and growth studies are important to understand and control the vitrification of liquids, as well as to develop new glass-ceramics having unusual properties and applications.

While all glasses display surface crystallization when properly heated, only a few show internal nucleation in the absence of nucleating agents. These few systems are of primary interest to study and test nucleation and overall crystallization theories. Recently, Fokin et al. [1] summarized nucleation data for the known oxide glasses that nucleate in the volume. These comprise only some stoichiometric compositions, e.g. $Na_2O \cdot 2CaO \cdot 3SiO_2$, $2Na_2O \cdot CaO \cdot 3SiO_2$, $Li_2O \cdot 2SiO_2$, $BaO \cdot 2SiO_2$ and $CaO \cdot SiO_2$.

We will show in this article that fresnoite glass ($2BaO \cdot TiO_2 \cdot 2SiO_2$) is an additional system showing internal crystallization, which displays the highest nucleation rates reported for inorganic glasses.

Keding and Rüssel [2] induced crystallization in a series of non-stoichiometric fresnoite-like glasses

* Corresponding author.
E-mail address: acabraljr@cefet-ma.br (A.A. Cabral).
[1] On sabbatical leave from S.I.Vavilov's State Optical Institute, 36-1 Babushkina, St. Petersburg 193171, Russia.

0022-3093/$ - see front matter © 2003 Published by Elsevier B.V.
doi:10.1016/j.jnoncrysol.2003.08.046

by electrochemical methods and obtained highly oriented fresnoite glass-ceramics, which have interesting electrical properties. Preliminary experiments of Keding [3] by traditional methods, such as DSC and optical microscopy, demonstrated that internal crystallization occurred in stoichiometric fresnoite glass. However, due to its fast crystallization, it was difficult to quantify the crystallization kinetics in that glass by such conventional techniques. Hence, no quantitative data were obtained in Ref. [3].

The aim of this work is to systematically measure the internal crystal nucleation and crystal growth rates in almost stoichiometric fresnoite glass. As this composition shows polymorphic crystallization it can be used to test nucleation theories. One such test will be the subject of Part II of this paper.

2. Literature review

A comprehensive literature search shows several studies about fresnoite single and polycrystals. Fresnoite single crystals can be grown using the Czochralski technique. Thus some of its physical properties have been measured [4–7]. Due to its interesting properties and stability at high temperatures, high tech applications have been suggested for this material, for instance in ultra-sonic devices and high frequency units, such as generators and sensors. These studies gave impetus to search for fresnoite glass-ceramics, which, in principle, are easier to produce than single crystals.

Structural characterization of glassy and polycrystalline fresnoite has been carried out by a series of traditional techniques, such as XRD (X-ray diffraction) [8–11], Raman spectroscopy and microRaman spectroscopy [11–13], and more sophisticated methods, such as XANES (X-ray absorption spectroscopy near-edge structure) [14,15] and XPS (X-ray photoelectron spectroscopy) [16]. It has been observed that Ti^{+5} is the dominant Ti species in fresnoite glass and polycrystalline structures, but Ti^{+4} and Ti^{+6} are also present.

Fresnoite glass-ceramic has attracted specialists' interests due to its behavior as a polar material that does not have an inversion center, in which non-ferroelectric crystalline phases can be oriented during crystallization, leading to excellent pyroelectric and piezo-electric properties. Highly oriented glass-ceramics can be obtained due to the existing permanent dipole moment in fresnoite. Such glass-ceramics have been obtained by two methods. The first one consists in inducing surface crystallization with subsequent textured growth towards the specimens center, as demonstrated by Halliyal et al. [4,17,18]. In the second one, glass-ceramics are prepared by electrochemical nucleation of melts, with electrodes inserted into a glass melt and a dc-potential of a few eV applied [2].

Ray and Day [19] studied by DSC the crystallization kinetics of glasses with molar compositions $1/2(100-x)\mathrm{BaO}\cdot 1/2(100-x)\mathrm{TiO_2}\cdot x\mathrm{SiO_2}$, with $x = 20$, 25, 30, 33 and 40. They observed that the apparent activation energy for overall crystallization decreases from 325 to 250 kJ/mol with increasing x.

This brief review demonstrates that there is some information about the crystalline structure and physical properties of fresnoite crystals and glass, but no report is available about crystal nucleation, growth and overall crystallization kinetics of stoichiometric fresnoite glass.

3. Theory

It is well known that on cooling a melt or reheating a glass, crystal nucleation can occur homogeneously or heterogeneously. The classical nucleation theory (CNT) for condensed systems, derived by Turnbull and Fischer [20] in the late 40's, is often used to understand and predict nucleation rates in undercooled melts. The subsequent step, crystal growth of internally distributed nuclei can lead to glass-ceramics.

Overall crystallization occurs by a combination of nucleation and growth. The kinetics of such process is usually described by a theory derived independently, in the late 1930s by Kolmogorov [21], Johnson and Mehl [22] and Avrami [23–25], best known as Kolmogorov–Avrami or Johnson–Mehl–Avrami theory, hereafter denominated JMAK theory. If the conditions on which the

JMAK theory was derived are not violated, the volume fraction transformed as a function of time, $\alpha(t)$, in isothermal conditions, is given by

$$\alpha(t) = 1 - \exp\left[- g \int_0^t I(t') \left[\int_{t'}^t U(t)\,\mathrm{d}t \right]^3 \mathrm{d}t' \right], \tag{1}$$

where g is a shape factor, which is equal to $4\pi/3$ for spherical crystals, and I and U are the crystal nucleation and growth rate, respectively.

This equation takes up two limiting forms. For constant crystal nucleation and growth rates throughout the transformation (homogeneous nucleation), Eq. (1) can be expressed by

$$\alpha = 1 - \exp\left(- \frac{gIU^3t^4}{4} \right). \tag{2}$$

If the induction periods for nucleation, t_{ind}, are significant, then, to a first approximation, t should be replaced by $(t - t_{\mathrm{ind}})$ in the above equations.

On the other hand, if the number of growing crystals does not change, e.g. all nucleation centers are exhausted at an early stage of transformation due to fast heterogeneous nucleation, crystal growth occurs from a fixed number of sites and the limiting value of Eq. (1) is then

$$\alpha = 1 - \exp(-gNU^3t^3), \tag{3}$$

where N is the number of sites per unit volume.

Avrami has proposed that for three-dimensional nucleation and growth processes, the following general relation should be used:

$$\alpha = 1 - \exp(-Kt^m), \tag{4}$$

where $3 \leqslant m \leqslant 4$. This expression covers all cases where I is a function of time, up to the limit when I is constant. It also covers the case of heterogeneous nucleation from a constant number of sites, which are activated at a constant rate till becoming depleted at some intermediate stage of the transformation.

Eq. (4) is usually linearized and takes the following form:

$$\ln(-(\ln(1-\alpha))) = \ln K + m \ln t. \tag{5}$$

Therefore, the so called Avrami coefficient, m, can be calculated from the slope of a $\ln[-\ln(1-\alpha)]$ versus $\ln(t)$ plot. The linearity of such plot is taken as an indication of the validity of the JMAK equation for the case under study.

When homogeneous nucleation is the operative mechanism, one can also use the y-axis intercept of such plot, $\ln(K)$, to compute the crystal nucleation rates, i.e. $I = 3K/\pi U^3$.

Thereby, Eq. (5) will be used to infer the crystallization mechanism of fresnoite glass and to estimate the nucleation rates.

4. Experimental procedures

The glass was prepared in an inductively heated furnace at the Otto-Schott Institute, Jena – Germany. Chemical analyses are shown in Table 1. The glass composition is quite close to the stoichiometric, especially if one takes into account that 2% error is typical in wet chemical analysis.

Glasses and crystalline products were characterized using differential scanning calorimetry and X-ray diffraction. Heat treatments were carried out in a tubular furnace with a central zone kept within ±1 °C. Due to its extremely high crystal nucleation rates the specimens were subjected to single-stage heat treatment schedules, instead of the conventional two-step treatments.

In order to find out the most appropriated temperature range for heat treatments, a DSC run of the fresnoite glass was carried out. The onset glass transition temperature, the exothermic crystallization peak and the melting point obtained were approximately 708, 800 and 1440 °C, respectively. Table 2 shows the treatment temperatures and times used in this study.

The viscosity curve, $\eta(T)$, was only measured at temperatures close to the melting point. Due to the fast crystallization on the cooling path, it was not possible to prepare bulk samples for measurements around T_g. Nevertheless, as the viscosity is $\sim 10^{12.5}$

Table 1
Chemical analysis of fresnoite glass (mol%)

	BaO	SiO_2	TiO_2
Nominal	40.0	40.0	20.0
B_2TS_2 glass	41.3	39.4	19.4

Table 2
Heat treatment temperatures and times used for crystal nucleation rates and crystal growth rates measurements

T (°C)	t (min)
680	35, 38, 40, 42, 45, 48, 50 (h)
710	150, 170, 180, 190, 200
720	70, 80, 90, 100, 110
730	30, 40, 50, 60, 70
735	20, 30, 40, 50
740	20, 30, 40
750	5, 10, 15, 20

Pa s at T_g, we fitted this value together with the high temperature data using the VFT equation. Then, the following equation was obtained:

$$\log \eta = -2.92 + \frac{1767.26}{T - 866.37}, \quad (6)$$

where T is the absolute temperature and the viscosity is given in Pa s.

The VFT equation corresponds to temperature dependent activation energy for viscous flow. Nevertheless, in a short temperature interval one can treat viscosity as Arrhenian. Fig. 1 shows the $\ln(\eta/T)^{-1}$ versus $1/T$ plot for the temperature range used in the present work (680–750 °C). The line slope corresponds to an activation enthalpy of $\Delta H_\eta = 294 \pm 23$ kJ/mol.

We used the XRD technique to estimate the crystallized volume fraction. A fully crystallized glass (treated at 740 °C for 20 h) was used as a standard. The intensities of the six main diffraction peaks, indicated on Fig. 2, were compared with standard patterns. Only fresnoite lines were detected.

The number and size of the crystals were measured through scanning electron microscopy (SEM) with a magnification of 50,000×. The experimental procedures were divided into the following basic steps. In the first, the heat-treated samples were polished and etched with a 0.8% HF–0.2% HCl solution and cleaned with ultra sound. Next, standard procedures, as described by Vogel et al. [26], were used to prepare the surfaces for the SEM studies. Finally, commercial software for image analysis was used to count the number of crystals per unit of area and to measure the crystal sizes.

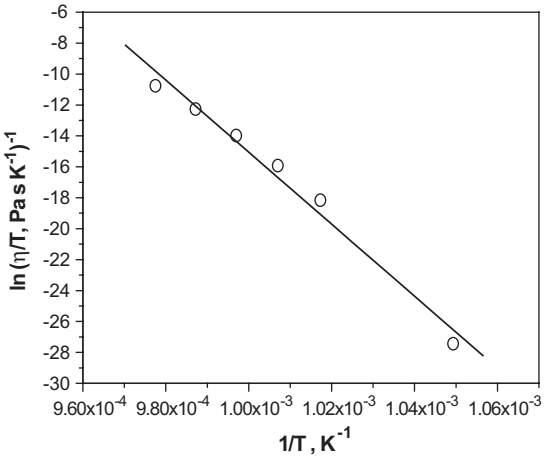

Fig. 1. $\ln(\eta/T)^{-1}$ as a function of the reverse temperature for a fresnoite glass. The points were calculated using the corresponding VFT equation.

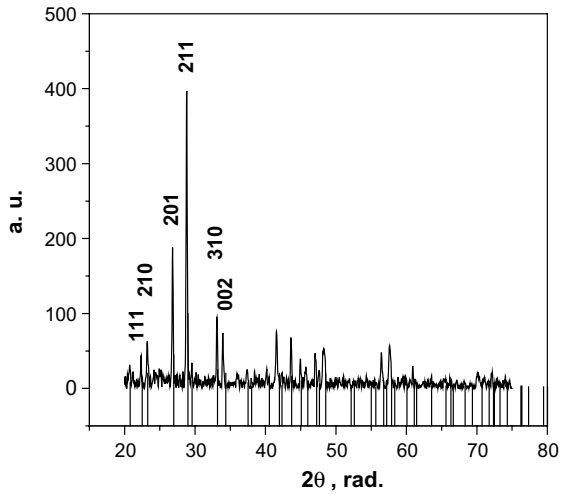

Fig. 2. XRD-patterns of a sample fully crystallized at 740 °C during 20 h with the composition of $2BaO \cdot TiO_2 \cdot 2SiO_2$. The straight lines are from JCPDS data base (card number 22-0513).

As the shape of the fresnoite crystals resembles prolate ellipsoids, following Ref. [27], we replaced the term U^3 in Eqs. (2) and (3) by the product $U_{max}U_{min}^2$ to analyze the overall crystallization kinetics. U_{max} and U_{min} are the crystal growth rates obtained from the time evolution of the major and minor radius of the largest crystals, respectively.

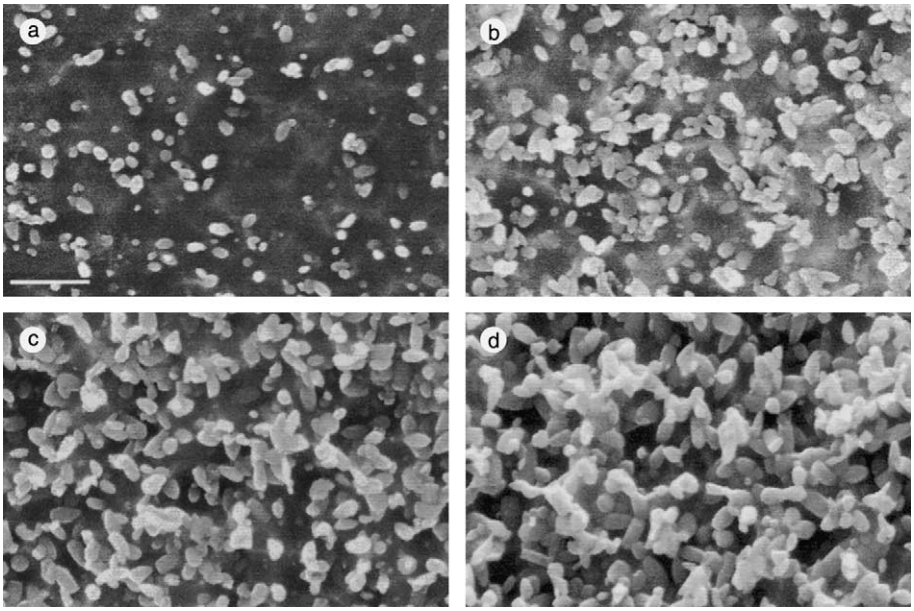

Fig. 3. Evolution of the number, size and fraction of crystals observed by SEM for the fresonite glass heat treated at 720 °C during: 70 (a); 90 (b); 100 (c) and (d) 110 min. The bar showed in (a) corresponds to 1 μm.

5. Results

5.1. Crystal growth rates

Typical SEM micrographs are presented in Fig. 3. The crystals have ellipsoidal shape. [2] The number of crystals and their sizes continuously increase with heat treatment time, indicating simultaneous crystal nucleation and growth.

The major, R_{max}, and minor, R_{min}, radius of the largest crystals (the crystals that first nucleated) were measured from similar micrographs.

Fig. 4(a)–(g) show R_{max} and R_{min} as a function of time for several temperatures. The equations of the resulting kinetic curves were obtained by a least-squares linear fit to each data set; whose intercepts and slopes yield the induction period for crystal growth (t_{gr}) and crystal growth rates (U_{max} and U_{min}), respectively.

[2] The collection of ellipsoidal fruit seed like crystals in heat treated fresnoite glass were baptised here as 'papaya microstructures'.

Arrhenius behavior is observed in Fig. 5 (in this limited temperature range, 680–750 °C) in $\ln(U)$ versus $1/T$ plots. Thus the crystal growth rates clearly increase with temperature. The slope of these Arrhenius plots corresponds to an activation enthalpy $\Delta H_U = 61 \pm 3$ kJ/mol.

The temperature dependence of t_{gr} is demonstrated in Fig. 6, as $\ln(t_{gr})$ versus $1/T$. Since the values of t_{gr} were obtained from the extrapolation of experimental $R(t)$ plots back to $R = 0$, it is reasonable to treat this time as that required to form the first critical nucleus, a quantity that can be close to the induction period for nucleation [28], as it will be discussed in the next part.

5.2. Crystal nucleation

5.2.1. Crystal nucleation rates estimated from the overall crystallization kinetics

Fig. 7(a)–(e) show the experimental crystallinity measured by XRD at 680, 720, 730, 740 and 750 °C ($T_g = 708$ °C).

In order to infer the crystallization mechanism, Avrami plots were constructed for each tempera-

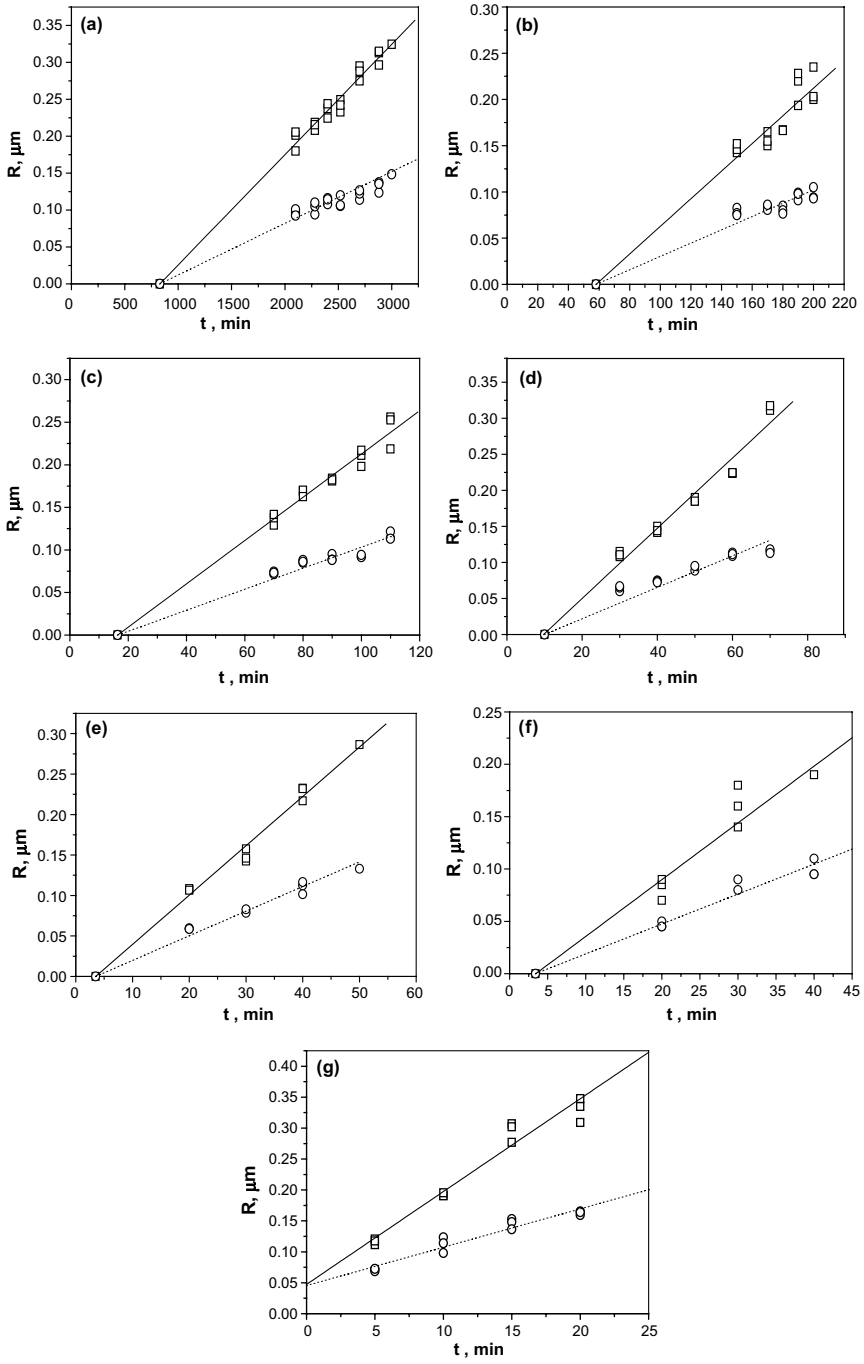

Fig. 4. Radius of the fresnoite ellipsoidal crystals (major (□) and minor axes (○)) as a function of the heat treatment time at the following temperatures (a) 680 °C; (b) 710 °C; (c) 720 °C; (d) 730 °C; (e) 735 °C; (f) 740 °C; (g) 750 °C. The lines correspond to the least-squares fit.

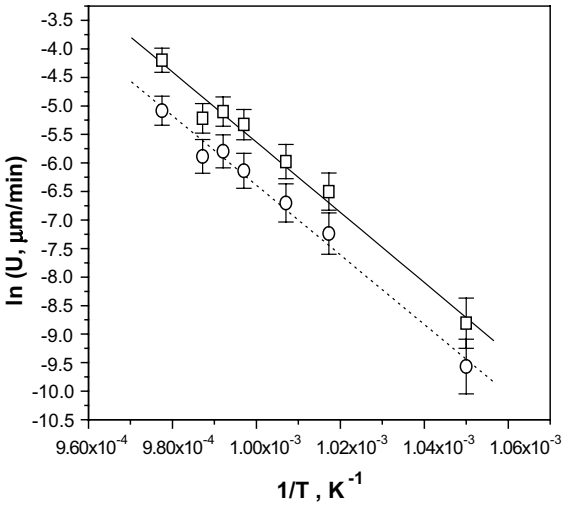

Fig. 5. Arrhenius plots of the crystal growth rates measured from major (□) and minor (○) axes. The lines correspond to the least-squares fit obtained for each data set.

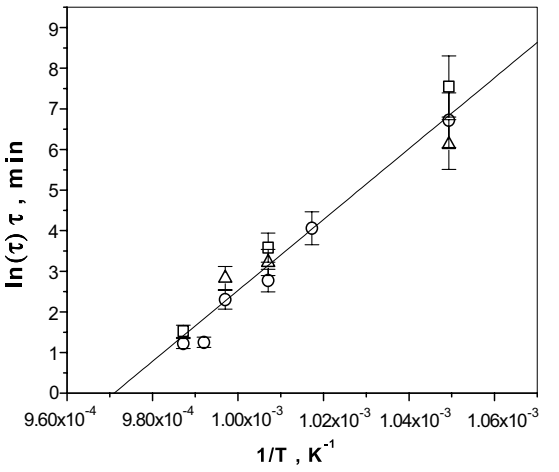

Fig. 6. Induction period obtained from the following plots: (○) $R(t)$; (△) $\alpha(t)$; and (□) $N(t)$, as a function of the reverse temperature. The line corresponds to the least-squares fit obtained if one assumes these points as a whole.

ture through Eq. (5), as demonstrated by the inset of Fig. 7. When there is an induction period for crystal growth, t_{ind} was replaced by t_{gr} in a $\ln[-\ln(1-\alpha)]$ versus $\ln(t-t_{gr})$ plot. Except for 750 °C, the slopes obtained for each temperature were within the range 3.8 ± 0.2. Then, m clearly tends to 4, indicating that crystallization in fresnoite glass occurs by simultaneous nucleation and growth with constant rates. This conclusion is corroborated by the fact that the experimental crystal nucleation and growth plots are linear and time independent.

For homogeneous nucleation, Eq. (4) assume the following general form:

$$\alpha = 1 - \exp(-K(t - t^J_{ind})^4), \tag{7}$$

where K and t^J_{ind} are fit parameters. Therefore, from crystallized volume fraction data these two adjustable parameters are obtained. From K and the corresponding crystal growth rates it is possible to compute crystal nucleation rates, hereafter denominated I^J.

Fitted results were used to plot the solid lines in Fig. 7(a)–(d) for the following temperatures: 680, 720, 730 and 740 °C. The temperature dependencies of the time lag, $\tau = 6t^J_{ind}/\pi^2$, calculated from t^J_{ind}, and nucleation rate, calculated from K, are presented in Figs. 6 and 8, respectively. Fig. 6 shows a strong temperature dependence of the time lags (that were estimated in different ways).

The value of m for 750 °C is close to 3 (inset in Fig. 7(e)). According to Avrami [23–25], this value indicates that at this temperature crystal growth starts from pre-existing nuclei. In fact, Table 2 shows that the shortest heat treatment time (5 min) employed is approximately equal to the time period that the furnace takes to stabilize after inserting the sample, which favors the appearance of nuclei during this time.

To test this possibility an Avrami plot was constructed using $m = 3$. From the resulting intercept ($K = 4\pi/3N_0U_{max}U^2_{min}$), the number of pre-existent nuclei, N_0, was computed by using the corresponding crystal growth rates. As result, we obtained $N_0 = 33$ crystals/μ^3. However, it is possible that, at this temperature, new crystals form as the heat treatment time increases. Then, one needs to take into account the growth of the pre-existing crystals plus the newly formed crystals. In this case, assuming constant nucleation and growth rates, in isothermal conditions, Eq. (1) must be rewritten as

$$\alpha = 1 - \exp\left(-\frac{\pi I U_{max} U^2_{min} t^4}{3} - \frac{4\pi N_0 U_{max} U^2_{min} t^3}{3}\right), \tag{8}$$

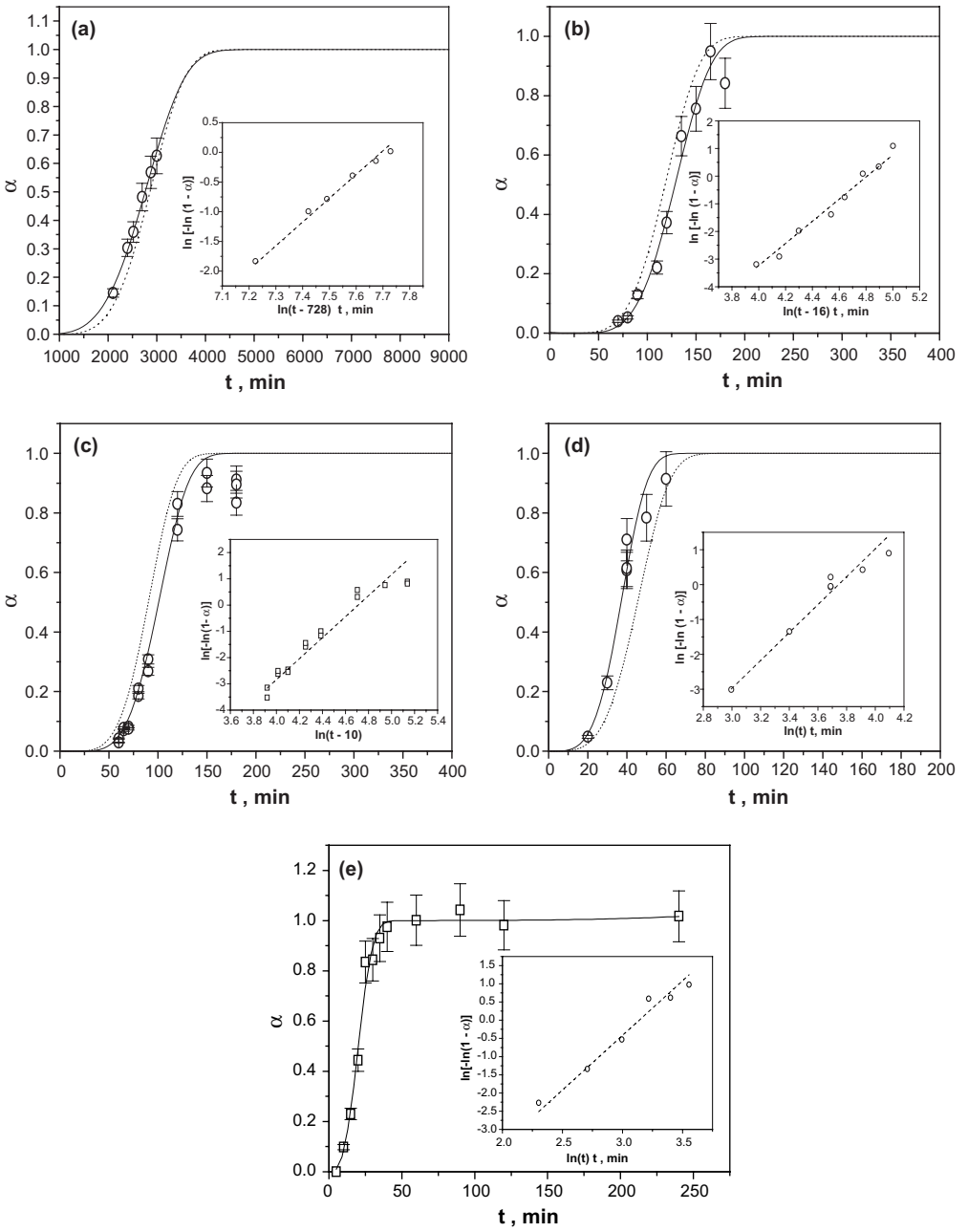

Fig. 7. Time evolution of the crystallized fraction measured from XRD for the following temperatures: 680 (a); 720 (b); 730 (c); (d) 740 and (e) 750 °C. The solid lines correspond to the fit of Eq. (7), using K and t_{ind}^{J} (see text) solid lines. The dot lines were fitted using t_{gr} and I^{*}, which was obtained from $N^{*}(t)$ plots. Inset shows the corresponding $\ln[\ln(1-\alpha)^{-1}]$ versus $\ln(t)$ plots (Eq. (5)), which were plotted as dashed lines. The error bars refer to the experimental errors detected for the volume fraction.

where the first and second terms in the exponential take into account the number of crystals formed during the heat treatment and the number of pre-existing nuclei, respectively. Using this equation,

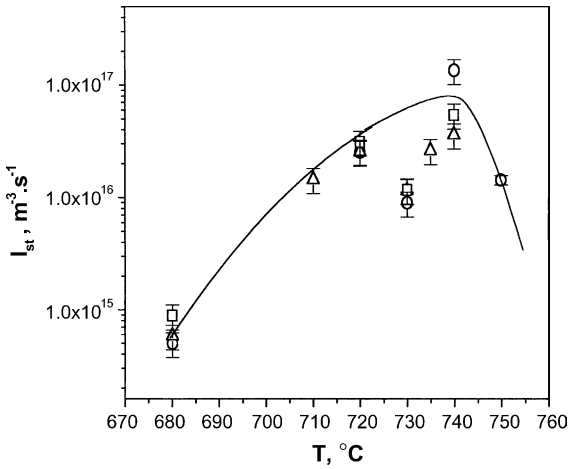

Fig. 8. Crystal nucleation rates as a function of temperature estimated from the following plots: (○) $\alpha(t)$; (△) $N_{vc}(t)$, and (□) $N^*(t)$. The line is only a guide for eye. The error bars correspond to the standard deviation estimated from the slopes of $N(t)$ plots.

we fitted a solid line in Fig. 7(e) and estimated $N_0 = 29\ \mu m^{-3}$ and $I = 1.4 \times 10^{16}\ m^{-3}\,s^{-1}$ at 750 °C.

5.2.2. Crystal nucleation densities estimated from the SEM micrographs

In order to evaluate the crystal nucleation rate, $I = dN_v/dt$, one must know the number density of crystals, N_v, from SEM micrographs. In the present case such determination is not trivial, since the etching procedure does not provide a flat surface where sectioned crystals can be observed (see Fig. 3). Nevertheless, we can use the following model for a rough estimation of N_v. According to the sketch shown in Fig. 9, the majority of the observed crystals contact the glass/gas interface, which we treat as being flat. However, one should bear in mind the crystals shown in gray and black on the sketch. The first type of crystals has no direct contacts with the glass surface, while the crystals of the second type cannot be observed. It is thus assumed that an underestimation of N_s owing to crystals of second type is in part compensated by an overestimation of N_s owing to crystals of the first type. Then, the number of observed crystals is close to that of the virtual crystal sections, N_s.

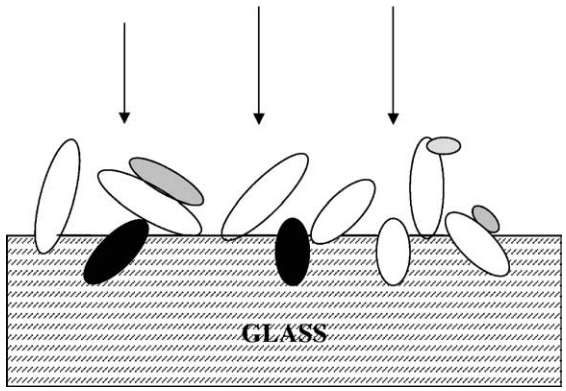

Fig. 9. Sketch of the heat-treated glass surface after the etching procedure used to prepare samples for SEM.

Hence we can use a precise expression that relates the number of crystals per unit volume, N_v, to the number of sectioned crystals in the specimen cross-section. For mono-dispersed systems of prolate ellipsoid shaped crystals the following equation was derived [29]:

$$N_v = \frac{N_s}{K_p(q)D_{min}}, \tag{9}$$

where N_s is the average number of crystals per unit area, $K_p(q \equiv D_{min}/D_{max})$ is a factor shape valid for prolate ellipsoids, and D_{min} and D_{max} are the largest crystal diameters measured from the minor and largest axes, respectively, revealed by our etching procedure.

For crystal size distributions resulting from simultaneous nucleation and growth with constant rates, one can rewrite Eq. (9) as [30]

$$N_v = \frac{2N_s}{K_p(q)D_{min}}. \tag{10}$$

According to Zanotto and James [31], single-stage heat treatments (as those used here) lead to an underestimation of the nucleation densities, since a certain fraction of the crystals, f, will be too small to observe in the SEM. The fraction lost is given by

$$f = \frac{\varepsilon}{R_{max}}, \tag{11}$$

where ε and R_{max} correspond to the microscopy resolution limit and the highest crystal radius of

the distribution, respectively. Then, a corrected number of crystals per unit of volume, denominated $N_{vc} = N_v(1 + f)$, was evaluated.

For the typical double-stage treatments, frequently reported in the literature, the glass samples are heat-treated separately for nucleation and growth. In that case, during the nucleation treatment the crystals normally do not attain measurable sizes and their contribution to the overall volume fraction transformed is negligible. However, our samples were subjected to long single-stage treatments. In this case, the chosen temperatures and times were enough to promote simultaneous nucleation and growth leading to substantial decrease of the glass matrix. Then, we have to take into account a second correction, i.e. the reduced volume of the amorphous phase.

To a first approximation, the average volume of glass for a heat treatment time t is

$$\frac{[1 + (1 - \alpha(t))]}{2} = 1 - \frac{\alpha(t)}{2}. \tag{12}$$

Then, we have to introduce a corrected crystal number density, given by

$$N^* = \frac{N_{vc}}{\left(1 - \frac{\alpha(t)}{2}\right)}. \tag{13}$$

Fig. 10(a)–(f) show the $N_{vc}(t)$ plots for the following temperatures: 680, 710, 720, 730, 735 and 740 °C. Except for 710 and 735 °C, we also calculated $N^*(t)$ and presented the results in the same plot. Using a least square fit, two lines were plotted to estimate the steady-state nucleation rate. The solid lines correspond to the $N_{vc}(t)$, while the dot ones are related to $N^*(t)$.

The values of the induction time for nucleation and steady-state nucleation rate obtained from $N^*(t)$ plots are presented in Figs. 6 and 8, respectively. For 710 and 735 °C, these kinetic parameters were only obtained from $N_{vc}(t)$ plots.

The dot lines in Fig. 7(a)–(d) represent $\alpha(t)$ plots calculated from the I_{st}, t_{ind} and U (obtained from SEM micrographs). These lines show a systematic deviation from the experimental points. This can be explained by the difference between I^*_{st} and I^J_{st}, and t_{gr} and t^J_{ind}.

6. Discussion

The main objective of this work was to develop a technique to gather nucleation data for a stoichiometric glass forming system that displays extremely high nucleation rates.

The basic parameters characterizing the nucleation process; i.e. nucleation time lag, τ, and steady-state nucleation rate, I_{st}, are presented in Figs. 6 and 8. The values of the time lag, directly estimated from $N_{vc}(t)$ plots, are in good agreement with those estimated from crystal growth kinetics, $R(t)$, as well as with those calculated from the overall crystallization kinetics (Fig. 6). In the restrict temperature range used here (680–750 °C) the decrease in time lag with increasing temperature is well described by an Arrhenius plot with an activation enthalpy $\Delta H_\tau = 87 \pm 6$ kJ/mol.

Apparent induction times may appear in $R(t)$ plots if the glass matrix or crystals suffer compositional shifts with time or some metastable phase (with lower growth rate) precipitates in the early stages of crystallization; however, there is no evidence for compositional shifts or metastable phase formation in this glass. A third possibility is that one is measuring crystals of a size range for which U is yet size dependent. However, as demonstrated by Kelton and Greer [32], the growth rate almost reaches steady-state at $R \sim 5R^*$. Then, as the smallest (measured) fresnoite crystals had radii of about 50 nm, we were probably outside this size dependent range. Therefore, t_{gr} probably reflects the time required to form the first critical nuclei.

Despite the approximations used to estimate the crystal nucleation rate from SEM micrographs, reasonable agreement is observed between the steady-state nucleation rates obtained from the slope of $N_{vc}(t)$ plots and those calculated from fitting to the JMAK equation (using the experimental crystal growth rate and $\alpha(t)$ curves).

The shape of the $I_{st}(T)$ dependence is typical of the Tammann nucleation maximum, resulting from a decrease of the thermodynamic barrier and increase of the kinetic barrier with decreasing temperature.

The value of the nucleation rate maximum, $I_{max} \equiv I_{st}(T_{max}) \cong 10^{17}$ m^{-3} s^{-1}, at the peak of the $I_{st}(T)$ curve has engaged our principal attention.

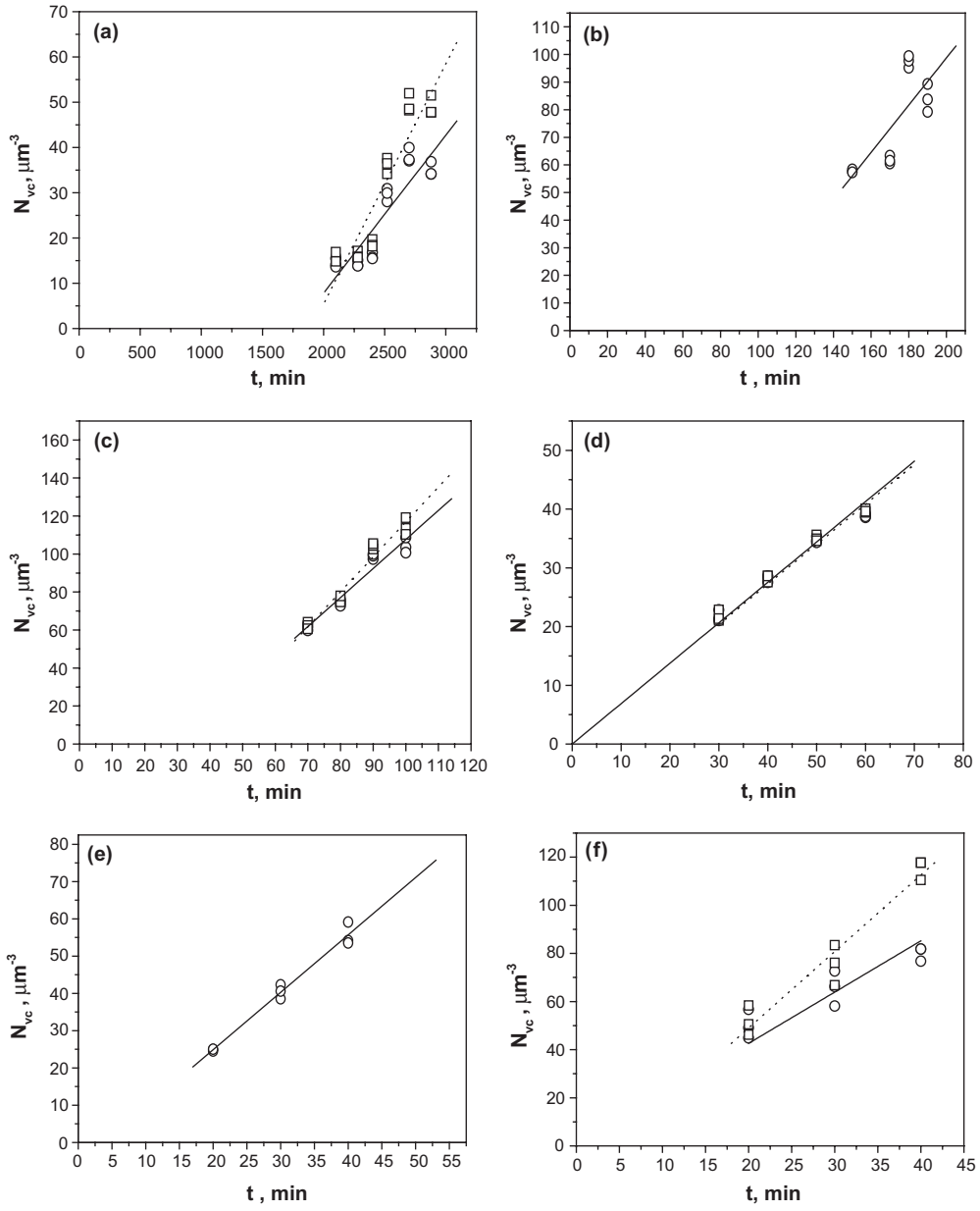

Fig. 10. Crystal nucleation densities as a function of time obtained for following temperatures: (a) 680 °C; (b) 710 °C; (c) 720 °C; (d) 730 °C; (e) 735 °C and (f) 740 °C. The solid lines correspond to the fit of the experimental points (○) estimated from $N_{vc} = N_v(1+f)$. The dot lines were fitted using the measurements (□) obtained through Eq. (13).

This value exceeds by ~4 orders of magnitude the highest I_{max} ever reported for silicate glasses ($\sim 4.3 \times 10^{13}$ m^{-3} s^{-1} for nucleation of $2Na_2O$–CaO–$3SiO_2$ crystals in a glass of the same composition) [33]. In fact, the I_{max} of fresnoite is comparable to those of some metallic glasses [34]. Thus, we extended the range of available nucleation rate data for silicate glasses to 16 orders

of magnitude, from the minimum value of $I_{max} \sim 10^{1.4}$ m^{-3} s^{-1} [35]. One now should explain what are the reasons for these extremely high nucleation rates in fresnoite glass. This will be performed in Part II of this article.

Finally, some comments about the activation enthalpy for viscous flow, ΔH_η, crystal growth, ΔH_U, and transport of structural units across the nucleus/melt interface, ΔH_τ. In the range of 680–750 °C, these values, calculated as the slopes of the respective Arrhenius plots, increase in the following sequence:

$$\Delta H_\eta = 294 > \Delta H_\tau = 87 > \Delta H_U = 61 \text{ kJ/mol}.$$

As demonstrated for a number of silicate glasses [33,36] the activation free energies, ΔG, for the mentioned above processes

$$\Delta G = \Delta H - T\Delta S \tag{14}$$

are similar, while their temperature dependencies ($\partial G/\partial T$), i.e. the activation entropies ($\Delta S = -\partial \Delta G/\partial T$), are distinguished $\Delta S_\eta > \Delta S_\tau > \Delta S_U$. As a result one obtains the same trend from Eq. (14), i.e. $\Delta H_\eta > \Delta H_\tau > \Delta H_U$.

7. Conclusions

We measured the internal, homogeneous, crystal nucleation rates, induction times, crystal growth rates and overall crystallization kinetics in almost stoichiometric fresnoite glass for the first time. Two methods were used to obtain the nucleation rates: directly from SEM micrographs and indirectly from the JMAK expression (using experimental crystallized fractions and crystal growth rates). The nucleation rates obtained by these two methods are in reasonable agreement and their temperature dependence peaks at $T_{max} > T_g$.

The time lags for nucleation obtained both from electron microscopy data and overall crystallization, consistently decrease with increasing temperature.

The activation enthalpy for viscous flow, ΔH_η, crystal growth, ΔH_U, and transport of structural units across the nucleus/melt interface, ΔH_τ, were estimated as $\Delta H_\eta = 294 > \Delta H_\tau = 87 > \Delta H_U = 61$ kJ/mol. This trend is similar to that found for other stoichiometric silicate glasses that nucleate internally.

The maximum nucleation rate in fresnoite glass ($\sim 10^{17}$ m^{-3} s^{-1}) is the highest so far measured in inorganic glasses. These data may be useful to further test nucleation theories.

Acknowledgements

The authors acknowledge the financial support provided by CAPES/PICDT, PRONEX and FAPESP. We also thank Drs Nora Diaz-Mora and Ralf Keding for preparing the glass, and Professor I. Avramov for useful suggestions.

References

[1] V.M. Fokin, E.D. Zanotto, J. Schmeltzer, J. Non-Cryst. Solids 321 (2003) 52.
[2] R. Keding, C. Russel, J. Non-Cryst. Solids 219 (1997) 136.
[3] R. Keding, Otto-Scott Institute, Jena, private communication (1996).
[4] A. Halliyal, A.S. Bhalla, S.A. Markgraf, R.E. Newnham, Ferroelectrics 62 (1985) 27.
[5] S. Haussühl, J. Eckestein, K. Recker, F. Wallrafen, J. Cryst. Growth 40 (1977) 200.
[6] Z.P. Chang, A.S. Bhalla, Mater. Lett. 8 (1989) 418.
[7] M.C. Foster, D.J. Arbogast, R.M. Nielson, P. Photinos, S.C. Abrahams, J. Appl. Phys. 85 (1999) 2299.
[8] J.T. Alfors, M.C. Stinson, R.A. Matthews, Am. Mineral. 50 (1965) 314.
[9] R. Masse, J.C. Grenier, A. Durif, Bull. Soc. fr. Minéral. Crystallogr. 90 (1967) 20.
[10] P.B. Moore, S.J. Louisnathan, Z. Kristallogr, 130 (1969) 438.
[11] S.A. Markgraf, A. Halliyal, A.S. Bhalla, R.E. Newnham, Ferroelectrics 62 (1985) 17.
[12] S.A. Markgraf, S.K. Sharma, A.S. Bhalla, J. Am. Ceram. Soc. 75 (1992) 2630.
[13] G.S. Henderson, M.E. Fleet, Can. Miner. 33 (1995) 399.
[14] F. Farges, J. Non-Cryst. Solids 204 (1996) 53.
[15] V. Mastelaro, R. Keding, J. Non-Cryst. Solids 282 (2001) 181.
[16] M. Schneider, W.O. Richter, R. Keding, C. Russel, J. Non-Cryst. Solids 226 (1998) 273.
[17] A. Halliyal, A.S. Bhalla, R.E. Newnham, L.E. Cross, J. Mater. Sci. 16 (1981) 1023.
[18] A. Halliyal, A.S. Bhalla, R.E. Newnham, Mater. Res. Bull. 18 (1983) 1007.
[19] C.S. Ray, D.E. Day, J. Am. Ceram. Soc. 67 (1984) 806.

[20] D. Turnbull, J.C. Fischer, J. Chem. Phys. 17 (1949) 71.
[21] A.N. Kolmogorov, Izv. Akad. Nauk. SSR 3 (1937) 355.
[22] W.A. Johnson, R. Mehl, Trans. AIME 135 (1939) 416.
[23] M. Avrami, J. Chem. Phys. 7 (1939) 1103.
[24] M. Avrami, J. Chem. Phys. 8 (1940) 212.
[25] M. Avrami, J. Chem. Phys. 8 (1941) 177.
[26] W. Vogel, L. Horn, H. Reiss, G. Völksch, J. Non-Cryst. Solids 49 (1982) 221.
[27] E.D. Zanotto, M.L.G. Leite, J. Non-Cryst. Solids 202 (1996) 142.
[28] I. Gutzow, Contemp. Phys. 21 (1980) 121, 243.
[29] R.T. Hoff, F.N. Rhines, Trans. Metall. Soc. 221 (1961) 975.
[30] A.M. Kalinina, V.M. Fokin, E.K. Shishkina, V.N. Filipovich, D.D. Dmitriev, Fiz. Khim. Stekla 9 (1983) 58.
[31] E.D. Zanotto, P.F. James, J. Non-Cryst. Solids 124 (1990) 86.
[32] K.F. Kelton, A.L. Greer, J. Non-Cryst. Solids 79 (1986) 295.
[33] V.M. Fokin, A.M. Kalinina, V.N. Filipovich, J. Cryst. Growth 52 (1980) 115.
[34] K.F. Kelton, Solid State Phys. 45 (1991) 75.
[35] J. Deubener, J. Non-Cryst. Solids 274 (2000) 195.
[36] N.D. Mora, E.D. Zanotto, V.M. Fokin, Phys. Chem. Glasses 39 (1998) 9.